ANALYZING RIM CREST VARIATIONS IN LUNAR IMPACT CRATERS. E. F. Lalor[1] and V. L. Sharpton[2]. [1]Dept. of Earth and Environmental Sciences, Temple University, Philadelphia, PA 19122 (eve.fattah@gmail.com), [2]Lunar and Planetary Institute, Houston, TX 77058 (sharpton@lpi.usra.edu).

Introduction: Cratering is the most common geologic process in the solar system. Understanding what controls crater shape [1-4] is therefore essential to using craters as exploration tools [5]. Though the impact process itself is generic, the variations in a crater are controlled by physical factors unique to the planetary body. On an airless body such as the moon, crater shape is controlled primarily by characteristics of the projectile (velocity, angle, mass) and the nature of the target (strength and gravity). Consequently, morphological variations in lunar craters give insight into lunar geology and the impact process.

Pike [2] compiled morphometric data on 484 lunar craters based on shadow measurements and topographic data from Apollo-era Lunar Topographic Orthophoto (LTO) maps. This dataset has provided the basis for widely used scaling relationships that are crucial to our current understanding of crater formation and for reliably using crater shape to constrain planetary stratigraphy (e.g., [5]). Here, we rely on high-resolution imagery and topography from the Lunar Reconnaissance Orbiter (LRO) to document the extent of rim height variations observed in morphologically fresh lunar craters, investigate the geologic controls over the observed variations, and evaluate the accuracy of Pike's [2] dataset using newly available high-resolution imagery and topography.

Methods: The GLD100 topographic dataset is a stereo-derived digital elevation model (DEM) from LRO Wide Angle Camera (WAC) imagery with a horizontal resolution of 100 m and vertical resolution of ±20 m [6]. Comparatively, the LTO maps used by Pike have a resolution of ±50 m vertical, ±200 m horizontal, and a contour interval of 100 m [4]. ESRI's ArcMap© was used for image processing and analysis.

Thirty morphologically fresh craters on mare plains were selected, ranging 9-42 km in diameter. Superposition on mare plains ensures ease of calculating the pre-impact surface. This size range includes simple and complex, and transitional craters. Craters smaller than ~5 km strain the resolution limits of GLD100, and larger craters are less common on the lunar mare and tend to be more heavily degraded.

The pre-impact surface was determined for use as the local elevation datum. For each crater, a local subset of the GLD100 was extracted. The elevation points of the crater and its ejecta were then removed from the local DEM and a trend surface was calculated from the remaining data points. The final DEM is referenced to the pre-impact surface of each crater.

The rim crest of each crater was traced to gain a polyline of X, Y, and Z coordinates every 100 meters around the circumference. The coordinates were used to calculate the radius at each vertex and its azimuth from the center. Elevation profiles were created extending clockwise around the rim of the crater (Fig. 1).

Discussion: For most craters, the average rim crest elevations from our study and the values reported by Pike [2] agree within 200 meters or less. We infer that resolution limits rather than methodical errors are the source of discrepancies in Pike's data. Overall, the measurements from LTO are more conformable than those from shadow measurements.

Pike's [2] data set was the basis for his depth-diameter (d/D) analysis in [3]. The d/D ratio is a function of increasing crater complexity. Simple craters are bowl-shaped with a d/D of roughly 1/5 [3], and complex craters are wider with flat, shallow floors and increasingly smaller d/D fractions. Pike [3] states that the simple to complex transition occurs at 16 km for lunar mare craters. In our analysis, no craters between 15 and 20 km could be confidently determined as either simple or complex, indicating that the transition is a spectrum rather than a binary.

The transition can be constrained by the degree of collapse that has occurred on the crater wall. Simple craters are small enough to be stable in their regular form and show minimal crest height or radial variation. The first transitional features observed are singular slump blocks that indicate local structural weaknesses, thus transitional craters show the greatest radial width variation due to asymmetric collapse. The degree of slumping escalates across the transitional zone. Complex craters are characterized by concentric terraces indicating that the entire wall has collapsed, and thus show the highest degree of crest height variability.

Anomalous simple craters are most likely influenced by target heterogeneities or impact obliquity (Fig. 1). The crater Mosting A (Fig. 1) is superposed on an interfingering of mare and highland lithologies. The less dense highland rock was preferentially excavated during impact, building an irregular rim crest. Messier crater (Fig. 1) is an exceptional example of an extremely low-angle impact. The uplift and ejecta are concentrated to the elongated crossrange walls, and are negligible in the uprange and downrange directions, showing a strong negative relationship between radius and rim height.

The first group of transitional craters has low height variability but high radial width variation. These

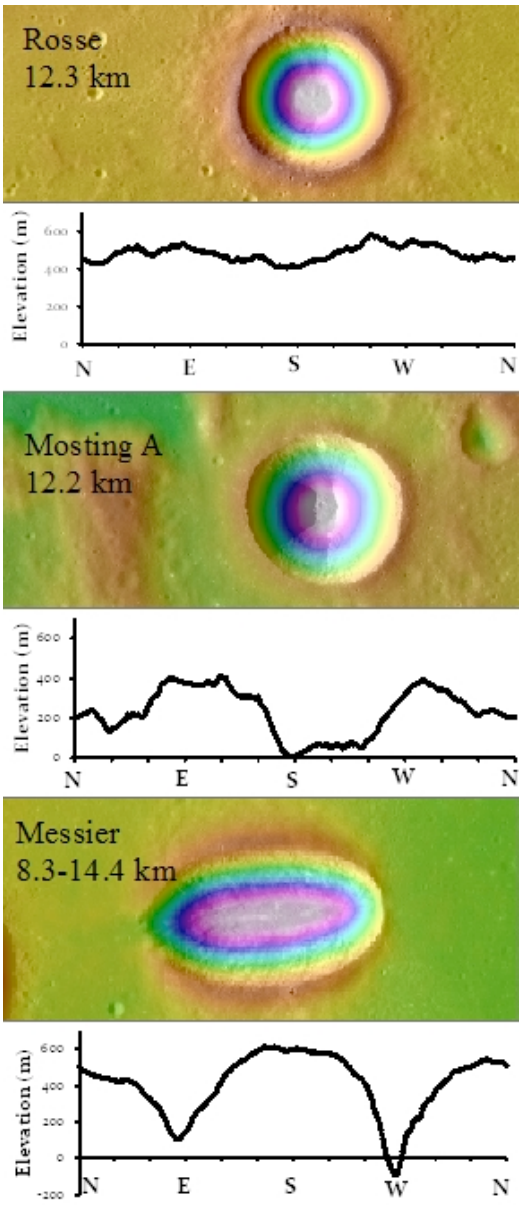

Figure 1: Simple Craters. Rosse crater (12.3 km) has a uniform rim crest with less than 200 m variance. Mosting A (12.2 km) has a variable rim crest reflecting the pre-impact topography. Messier (8.3-14.4 km) shows a predictable pattern of rim crest variation caused by low-angle impact.

craters have low degrees of circularity. In Carrel crater (Fig. 3A), the radius varies greatly due to a massive slump in the eastern quadrant of the crater. The localized slumping in such craters may indicate otherwise undetected structural weaknesses in the bedrock. The other set of transitional craters has high crest height variation and low radial variability. Flamsteed (Fig. 3B) exhibits broader sections of wall collapse, and this slumping contributes more to lowering the rim crest than to radial extension.

Formation of terraces within complex craters often coincides with a crenulated rim from multiple slumping events, as in Burg crater (Fig. 3C). These scalloped walls generate a wide range of crest height variations and reduce circularity. Picard (Fig. 3D) is anomalous as it is much smaller than other complex craters, has concentric terraces, yet maintains circularity and crest height regularity.

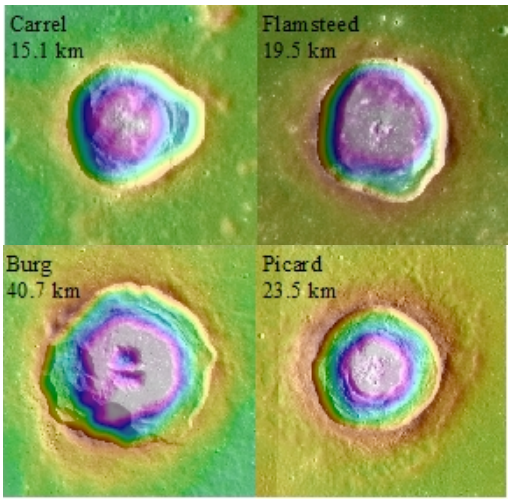

Figure 2: Transitional and complex craters. A. Carrel crater exhibits a singular slump block. B. The walls of Flamsteed have collapsed to a greater extent. C. Burg crater exhibits the characteristic scalloped rim of complex craters. D. Picard has maintained its roundness despite full rim collapse.

Conclusions: Modern remote sensing and ArcGIS analysis provide more precise measurements of the range of rim crest heights within lunar craters. Pike's [2] measurements reasonably agree with our average height values, though his shadow measurements show some significant deviations.

The transition from simple to complex crater morphology occurs over the 15-20 km range on the lunar mare surface in a stepwise addition of complex characteristics. As crater size and complexity increase, so do degrees of rim height and radius variation. Transitional craters show significant variability in either crest height or radius, both within individual craters and between craters of similar sizes. Complex craters have great rim crest disparities among themselves, but similar degrees of radial variation.

References: [1] Herrick, R. R. & Forsberg-Taylor, N. K. (2003) *Meteoritics & Planet. Sci. 38*, Nr 11, 1551-1578. [2] Pike, R. J. (1976) *The Moon, 15*, 463-477. [3] Pike, R. J. (1980) *Proc. Lunar Planet. Sci. Conf. 11th,* 2159-2189. [4] Settle, M. and Head, J.W. (1977) *Icarus, 31,* 123-135. [5] Dehon, R. A., & Waskom, J. A. (1975). *NASA STI/Recon Technical Report N*, *76*, 17001. [6] Scholten, F. et al. (2012) *JGR, 117,* E00H17.